Coupling light into and out from the surface plasmon polaritons of a nanometer-thin metal film with a metal nanostrip

Thomas Søndergaard,[1,*] Vahid Siahpoush,[2,3] and Jesper Jung[1]

[1]*Department of Physics and Nanotechnology, Aalborg University, Skjernvej 4A, DK-9220 Aalborg Øst, Denmark*

[2]*Laser-Plasma Research Institute, Shahid Beheshti University, G. C., Evin, Tehran 19839-63113, Iran*

[3]*Research Institute for Applied Physics, University of Tabriz, Tabriz 51665-163, Iran*

(Received 2 April 2012; revised manuscript received 16 August 2012; published 29 August 2012)

Scattering of light by a metal nanostrip placed near a nanometer-thin metal film in a homogeneous dielectric environment is considered. For a plane wave incident on the geometry from outside we study the scattering cross sections governing the excitation of symmetric and antisymmetric surface plasmon polariton (SPP) waves and out-of-plane (OUP) propagating waves. For a symmetric (long-range) or antisymmetric (short-range) SPP propagating along the metal film and being incident on the nanostrip, we study the fraction of power coupled into forward and backward propagating symmetric and antisymmetric SPP waves, and into OUP propagating waves, respectively. Resonance peaks in the scattering cross sections, or dips in the relative power going into all scattering channels due to resonant absorption, are related to standing-wave resonances of counterpropagating gap SPP waves in the gap between the metal nanostrip and the metal film. The resonances are studied with respect to the width of the metal nanostrip and the size of the gap between the metal film and nanostrip. For a 15-nm-thick film it is found that coupling of light in and out of the symmetric SPP is weak compared with coupling to and from OUP and antisymmetric SPP waves. Improving the in and out coupling of power in the symmetric SPP waves with thicker films (50 nm) and larger scattering objects is considered.

DOI: 10.1103/PhysRevB.86.085455 PACS number(s): 73.20.Mf, 71.36.+c, 02.30.Rz, 02.60.Cb

I. INTRODUCTION

A nanometer-thin metal film in a symmetric dielectric environment supports two types of electromagnetic waves known as symmetric (long-range) and antisymmetric (short-range) surface plasmon polaritons (S-SPPs and A-SPPs) that are bound to and propagating along the metal film.[1–4] The S-SPP waves have attracted considerable interest for waveguiding and passive optical components because their propagation losses can be greatly reduced by decreasing the film thickness. Propagation lengths of several millimeters, or even a few centimeters, is possible, which is equivalent to thousands of S-SPP wavelengths.[5–13] The long-range propagation is, however, achieved at the expense of weak confinement to the metal film. The S-SPP waves have, for example, been considered for directional couplers,[14,15] Y-splitters,[16] add-drop filters,[17] and reflection gratings.[18–20] The A-SPP waves on the other hand are much more strongly confined to the metal film and characterized by short propagation lengths. Due to the strong confinement it is also found that A-SPP waves are much more strongly reflected into backwards propagating A-SPP waves at film terminations, and strong resonances in optical antennas[21–23] can be explained as standing-wave resonances related to counterpropagating A-SPP waves reflected back and forth at film terminations.[24–26] A fundamental challenge for engineering of S-SPP or A-SPP devices, which is addressed in this paper, is the efficient and local coupling of light into and out from the SPP waves.

Coupling of light into ordinary single-metal-dielectric-interface SPP waves with a one-dimensional surface corrugation has been studied both theoretically and experimentally. A usual strategy for measuring the SPP wave excitation is to use a relatively thick silver or gold film, for example, a thickness of 40 nm, in an asymmetric dielectric environment with a small refractive index on one side of the film (e.g., air) and a larger refractive index on the other side (e.g., quartz). In that case the SPP waves confined to the air-metal interface will leak into the quartz substrate where their presence can be detected in the far field via leakage-radiation microscopy.[27–33] Another approach for detecting ordinary SPP waves is with fluorescence microscopy.[34] A well-documented geometry for coupling light into SPP waves is the grating coupler where an array of slits or ridges are used to scatter light into SPP waves.[35–38] Coupling of light out from ordinary single-metal-dielectric-interface SPP waves has been theoretically studied by approximations treating a small scatterer with the impedance boundary condition or with the method of reduced Rayleigh equations.[39–42] Scattering of ordinary SPP waves by one-dimensional scatterers has also been considered with a modal expansion technique[43–45] and with Green's function surface integral equation methods.[46–48]

In this paper we will study the coupling of light into and out from the S-SPP waves and A-SPP waves of a nanometer-thin metal film in a symmetric dielectric environment by scattering via a metal nanostrip placed nearby. The scattering situations considered in the paper are illustrated in Fig. 1. We will consider a geometry which is invariant along the z axis, that is, a two-dimensional geometry, where a silver nanostrip of width w and thickness d is placed a distance g above a planar silver film of thickness t. We consider p-polarized light propagating in the xy plane, that is, the magnetic field is of the form $\mathbf{H}(x,y,z) = \hat{z}H(x,y)$, where $\hat{z}$ is a unit vector along the z axis. The forward $(-)$ or backward $(+)$ propagating SPP waves can be described by a magnetic field of the form

$$H^{(i)}(x,y) = f_{(i)}(y)e^{\mp ik_{(i)}x}, \tag{1}$$

where i = S-SPP or A-SPP, and $f_{(i)}(y)$ is a function of y only being either symmetric or antisymmetric with respect to the midplane of the metal film. The magnetic-field distributions

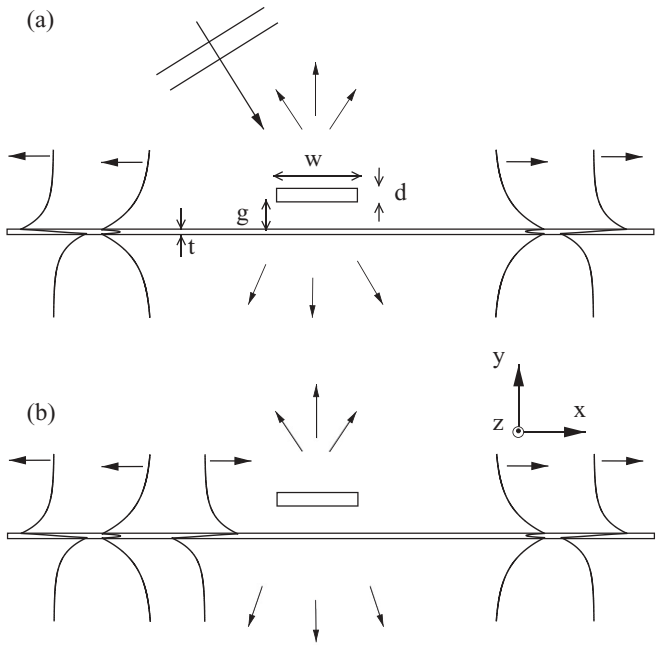

FIG. 1. Schematic of scattering configurations. (a) A plane wave is incident on a silver film of thickness t with a silver nanostrip of width w and thickness d placed a distance g above the film surface. Scattering of light into out-of-plane propagating waves and into forward and backward propagating symmetric and antisymmetric surface plasmon polaritons is illustrated. (b) An antisymmetric surface plasmon polariton propagating along the metal film is incident on the silver nanostrip, and is transmitted, reflected, or scattered into the same propagating wave channels as in (a).

for S-SPPs and A-SPPs calculated for the wavelength 633 nm and silver film thickness 50 nm are plotted in Fig. 1. We will study a scattering situation where a plane wave is incident on a silver film and silver nanostrip under an angle of incidence of 45° as illustrated in Fig. 1(a). This results in the excitation of forward (right) and backward (left) propagating S-SPPs and A-SPPs that are propagating away from the scattering silver nanostrip. In this geometry no SPP waves will be excited if the metal nanostrip is removed. Scattering by the metal nanostrip will also result in out-of-plane scattering, that is, scattered light propagating away from the metal film. Scattering of light into the different scattering channels will for this situation be quantified via the channel specific scattering cross sections. In particular, with the configuration in Fig. 1(a) we can study coupling of light into S-SPP and A-SPP waves. We will also consider the reverse scattering situation where an A-SPP [Fig. 1(b)] or S-SPP (not shown) is propagating along the metal film and being incident on the metal nanostrip. Here, due to scattering, the power in the incident SPP will be distributed between out-of-plane propagating waves, forward and backward propagating A-SPPs and S-SPPs, and light absorbed by the metal. This configuration allows studying coupling of light out from thin-film SPP waves.

The paper is organized as follows. In Sec. II the theoretical method that was used for calculating the scattering of light into each type of wave is outlined. The case of a 15-nm silver film with a 10-nm silver nanostrip close by is studied in Sec. III. The finding of an extremely small coupling of light into and out from S-SPP waves leads to a study of strategies to increase this in and out coupling by considering larger scattering objects (Sec. IV), and thicker metal films (Sec. V). Finally, we offer our conclusions in Sec. VI.

II. THEORETICAL METHOD

In a recent paper[49] the authors developed a Green's function approach for the case of a nanometer-thin metal film that allows for calculation of the excitation of S-SPPs and A-SPPs, and out-of-plane (OUP) propagating waves, respectively, from a magnetic line dipole source. In that approach the Green's function was split into different parts each governing the excitation of a certain type of wave, namely the excitation of S-SPPs, A-SPPs, and OUP waves, that is,

$$g(\mathbf{r},\mathbf{r}') = g^{\text{S-SPP}}(\mathbf{r},\mathbf{r}') + g^{\text{A-SPP}}(\mathbf{r},\mathbf{r}') + g^{\text{OUP}}(\mathbf{r},\mathbf{r}'), \quad (2)$$

where, for convenience, throughout this paper $\mathbf{r} = \hat{x}x + \hat{y}y$ with $\hat{x}$ and $\hat{y}$ being unit vectors along the x and y axes, respectively.

The results presented throughout this paper were obtained by applying the total Green's function $g(\mathbf{r},\mathbf{r}')$ from our previous paper[49] in the Green's function surface integral equation method, similar to what was done in Ref. 46 with another Green's function, to find the magnetic field $H(\mathbf{s})$ and its normal derivative $\hat{n}\cdot\nabla H(\mathbf{s})$ at the surface of the nanostrip in Fig. 1, where $\mathbf{s}$ is a position infinitesimally close to but outside the surface of the metal nanostrip, and $\hat{n}$ is the outward surface normal vector at that position. The effect of the surfaces of the metal film are automatically dealt with via the Green's function. Then the total magnetic field can be obtained at all other positions $\mathbf{r}$ outside the scatterer from those values found at the surface by the integral

$$H(\mathbf{r}) = H_0(\mathbf{r}) + \oint_C [H(\mathbf{s}')\hat{n}'\cdot\nabla' g(\mathbf{r},\mathbf{s}') - g(\mathbf{r},\mathbf{s}')\hat{n}'\cdot\nabla' H(\mathbf{s}')]dl', \quad (3)$$

where C is the surface of the nanostrip, and $H_0(\mathbf{r})$ is the field solution in the absence of the metal nanostrip. By replacing the total Green's function in this expression with each of the different parts of the Green's function we can straightforwardly decompose the scattered part of the total magnetic field into parts related to S-SPPs, A-SPPs, and OUP waves, that is, the calculated magnetic field can be decomposed in the following way:

$$H(\mathbf{r}) = H_0(\mathbf{r}) + H^{\text{S-SPP}}(\mathbf{r}) + H^{\text{A-SPP}}(\mathbf{r}) + H^{\text{OUP}}(\mathbf{r}). \quad (4)$$

For a position x to the right of the scattering object we can evaluate the power scattered into the forward propagating S-SPP and A-SPP by

$$P^{(i)} = \frac{1}{2}\mathrm{Re}\int_{y=-\infty}^{\infty} \mathbf{E}^{(i)}(x,y) \times [\mathbf{H}^{(i)}(x,y)]^* \cdot \hat{x}\, dy, \quad (5)$$

where $\mathbf{E}^{(i)}(\mathbf{r})$ is the corresponding electric field, and again i = S-SPP or A-SPP. To obtain the power scattered into the backward (left-) propagating S-SPPs and A-SPPs we can use a similar expression but with a choice of x located to the left of the scattering object, and by replacing $\hat{x}$ with $(-\hat{x})$. Note that in the case of a lossy metal the result will depend on x since the SPP waves are damped as they propagate. It is most convenient to work with the far-field expression for the parts of the Green's function $g^{\text{S-SPP}}$ and $g^{\text{A-SPP}}$ since an exact analytic expression in closed form exists.[49] For our purpose in this paper we will just note that the expressions are of the form

$$g^{(i),ff}(\mathbf{r},\mathbf{r}') = h_{(i)}(y,y')e^{-ik_{(i)}|x-x'|}, \quad (6)$$

where $k_{(i)}$ is the in-plane propagation constant of the respective type of SPP. Since these are straightforward analytic expressions that for $x > x'$ or $x < x'$ represent forward or backward propagating A-SPPs or S-SPPs, they can be inserted into Eq. (3) to obtain a far-field expression for the excitation of S-SPPs and A-SPPs, which when considering a position x lying either to the right or to the left of the scatterering nanostrip will be of the form of Eq. (1), in which case Eq. (5) for the power in the A-SPP or S-SPP becomes simply

$$P^{(i)} = \frac{1}{2}\mathrm{Re}\int_{y=-\infty}^{\infty} \frac{k_{(i)}}{\omega\varepsilon_0\varepsilon(x,y)}|H^{(i)}(x,y)|^2 dy, \quad (7)$$

where ε_0 is the vacuum permittivity, $\varepsilon(x,y)$ is the relative dielectric constant, and ω is the angular frequency. Since we know the propagation constant $k_{(i)}$ we can extrapolate backward from a position x in the far field to another position x being closer to the nanostrip to obtain the power in the A-SPP or S-SPP at that position instead. This procedure is entirely equivalent to just using the far-field expression for $g^{(i)}(\mathbf{r},\mathbf{r}')$ for the actual position x where we want to evaluate the power in the A-SPP or S-SPP. Note that if there are no absorption losses in the metal the power coupled into the respective types of SPPs will be independent of whatever x is chosen.

The power scattered into out-of-plane propagating waves is given by

$$\begin{aligned} P^{\text{OUP}} &= \frac{1}{2}\mathrm{Re}\oint \mathbf{E}^{\text{OUP}}(x,y) \times [\mathbf{H}^{\text{OUP}}(x,y)]^* \cdot \hat{n}\, dl \\ &= \frac{1}{2}\int \frac{k_0 n_1}{\omega\varepsilon_0\varepsilon_1}|H^{\text{OUP}}(r,\theta)|^2 r\, d\theta, \end{aligned} \quad (8)$$

where the integration path is a circle placed in the far field, $\hat{n}$ is the normal vector of the circle, and $\varepsilon_1 = n_1^2 = 1$ is the relative dielectric constant of the background material surrounding the metal film and strip, and $k_0 = 2\pi/\lambda$, where λ is the free-space wavelength. A simple analytic far-field expression in closed form for the out-of-plane part of the Green's function is also available (see Ref. 49) which can be used to straightforwardly obtain $H^{\text{OUP}}(\mathbf{r})$ in the far field when inserted in Eq. (3). Note that in the far field $H^{\text{OUP}}(r,\theta)$ is zero when $\theta = 0$ or π.[49]

When the silver nanostrip is illuminated with a p-polarized plane wave at an angle of incidence of θ_i relative to the x axis, that is, when the field incident on the whole geometry is

$$H_i(\mathbf{r}) = H_i e^{-ik_0 n_1[\cos(\theta_i)x - \sin(\theta_i)y]}, \quad (9)$$

we can define the scattering cross sections for power scattered into the different types of waves as the scattered power normalized with the power per unit area of the incident wave, that is,

$$\sigma^{(j)} = \frac{P^{(j)}}{\frac{1}{2}\frac{k_0 n_1}{\omega\varepsilon_0\varepsilon_1}|H_i|^2}, \quad (10)$$

where j = S-SPP, A-SPP, or OUP. Note that $H_0(\mathbf{r})$ is different from $H_i(\mathbf{r})$ and is the corresponding solution when the field $H_i(\mathbf{r})$ is incident on the metal film without the nanostrip.

When the incident field $H_0(\mathbf{r})$ is instead either an S-SPP or an A-SPP [see Eq. (1)] we can calculate the power P_0 of the incident SPP wave at a position x placed before the metal nanostrip by using Eq. (7) where here $H^{(i)}(\mathbf{r})$ must be replaced with $H_0(\mathbf{r})$. If, for example, the incident field is an A-SPP the power transmitted into a forward propagating A-SPP is given by now considering a position x on the other side of the scatterer and by inserting the total A-SPP field being $H_0(\mathbf{r}) + H^{\text{A-SPP}}(\mathbf{r})$ into Eq. (7) instead of just the scattered part. For all other scattering channels, either forward or backward propagating S-SPPs, the backward propagating A-SPP, or OUP propagating waves, the scattered power can be evaluated using the scattered fields in either Eq. (7) or (8). The fraction of power in each channel, forward and backward propagating A-SPPs and S-SPPs propagating away from the nanostrip, and OUP waves, can then be obtained by normalizing the power in each channel with the power of the incident wave. Note that the power in the S-SPP and A-SPP modes excited via scattering from the nanostrip will decrease as these modes propagate away from the nanostrip due to Ohmic losses in the metal film. Therefore the amount of power in these modes calculated using Eq. (7) will depend on the specific choice of x. Since the S-SPP and A-SPP waves only exist in the region outside the nanostrip, and we prefer to avoid the effect of propagation losses as much as possible when evaluating the coupling to various SPP waves, we will use a position x that is as close to the nanostrip as possible but still outside it, and on the appropriate side of it.

Note also that in a general case when there are absorption losses or material gain, the modes of a waveguiding structure are eigenmodes of a non-Hermitian operator, and contrary to the situation without absorption or gain, where power orthogonality is ensured by a Hermitian operator,[50] the power orthogonality or energy orthogonality between modes is no longer automatically ensured.[51] This can lead to interesting physics such as excess noise but could also mean that summing the power assigned to all individual modes could give a different result from the total power.[51] However, in our case the SPP modes are power orthogonal. This can be seen by inserting in an expression similar to Eq. (5) the electric field of an A-SPP, and the magnetic field of an S-SPP or vice versa, in which case the result is zero from symmetry considerations,

and thus there is no risk of counting the same power twice when using Eq. (5).

The results presented in the following sections have all been obtained with the procedure outlined above. For the calculations we have used the dielectric constant of silver from Ref. 52.

III. SCATTERING BY A NANOSTRIP ABOVE A 15-NM-THIN FILM

In this section we will study the scattering situations in Fig. 1 for a silver film of thickness $t = 15$ nm. The first case we will consider is a plane wave being incident under an angle of incidence of 45° on the silver film and nanostrip. The nanostrip is characterized by the width $w = 100$ nm, thickness $d = 10$ nm, and it is placed a distance $g = 10$ nm above the silver film [Fig. 1(a)]. The calculated scattering cross sections for the scattering channels of forward and backward propagating A-SPPs and S-SPPs, and OUP propagating waves, respectively, are presented in Fig. 2. It is striking that the S-SPP scattering cross sections are extremely small (<0.25 nm) compared with the A-SPP and OUP scattering cross sections. This is different from the excitation of A-SPPs and S-SPPs by a magnetic line dipole at similar distances to the metal film, where it was found that although the S-SPP excitation is smaller than the A-SPP excitation (at the wavelength 500 nm) the A-SPP-to-S-SPP power ratio is less than a factor of 10,[49] while here this ratio is approximately 242 at the wavelength 500 nm. On the other hand, in the scattering situations studied here the scattering cannot be expected to behave as the emission from a magnetic line dipole but will have more similarity with the emission from an electric line dipole. The confinement length of an SPP wave above the metal film can be defined as the distance above the film where the field magnitude has decreased by a factor e, that is, the confinement length is given by $L_{(i)} = 1/\mathrm{Re}(\sqrt{k_{(i)}^2 - k_0^2}) = \lambda/(2\pi \mathrm{Re}\sqrt{n_{(i)}^2 - 1})$, where $n_{(i)} = k_{(i)}/k_0$ is the mode index of the S-SPP or A-SPP. For the wavelength of 500 nm we find $L_{\text{S-SPP}} = 790$ nm and $L_{\text{A-SPP}} = 70$ nm, and for the wavelength of 1350 nm $L_{\text{S-SPP}} = 6330$ nm and $L_{\text{A-SPP}} = 690$ nm. Thus the thickness of the nanostrip is extremely small compared to the confinement length of the S-SPP, and much less so when compared with the A-SPP.

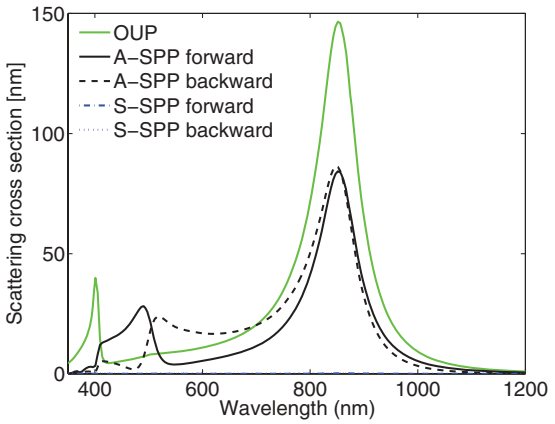

FIG. 2. (Color online) Channel specific scattering cross sections for the situation in Fig. 1(a) with $w = 100$ nm, $d = 10$ nm, $g = 10$ nm, and $t = 15$ nm. The angle of light incidence is 45°.

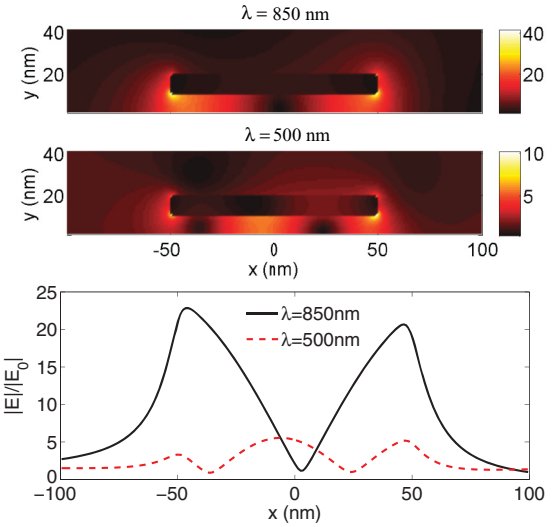

FIG. 3. (Color online) Normalized magnitude of electric field around the nanostrip for the situation in Fig. 2 at the resonance wavelengths 850 and 500 nm. Lower: Cross section of electric field magnitude through the middle of the gap between strip and film ($y = 5$ nm).

In the calculation of Fig. 2 the power in the respective SPP wave channels was evaluated at positions x just 1 nm to the left or the right of the nanostrip. Resonant scattering is visible at the wavelengths of 850 and 500 nm. The latter resonance is rather weak in the OUP cross section but still a small shoulder is noticeable. This resonance will be more easily identified later in Fig. 4. At the wavelength 850 nm the forward and backward A-SPP cross sections are similar, and when added together they exceed the OUP cross section, and they also exceed the physical cross section of the nanostrip. Thus, more than half of the scattered power is channeled into A-SPP waves. At the other resonance ($\lambda = 500$ nm) the forward and backward A-SPP cross sections are also similar but there is a transition, where increasing or decreasing the wavelength will cause one A-SPP cross section to dominate over the other. The nature of these resonances is revealed from field plots around the nanostrip (Fig. 3) showing the presence of standing wave resonances of different order related to counterpropagating gap SPP waves propagating back and forth in the gap between the metal film and strip and being reflected at the strip terminations. Similar resonances have previously been studied theoretically in Refs. 46, 47, and 53–55 for other scattering configurations. Gap-SPP resonators based on a nanometer-thin gap between two finite-length metal strips have also been realized experimentally.[56,57]

We will now consider the reverse situation [Fig. 1(b)] for the same geometry, where an A-SPP is incident on the nanostrip. Again the power in each SPP wave is evaluated at a position x being 1 nm to the left or to the right of the nanostrip. The power in each channel, forward and backward propagating S-SPP, backward propagating A-SPP (reflection), and forward propagating A-SPP (transmission), and OUP waves, is presented in Fig. 4. The transmission (A-SPP forward) has resonant transmission dips at the same

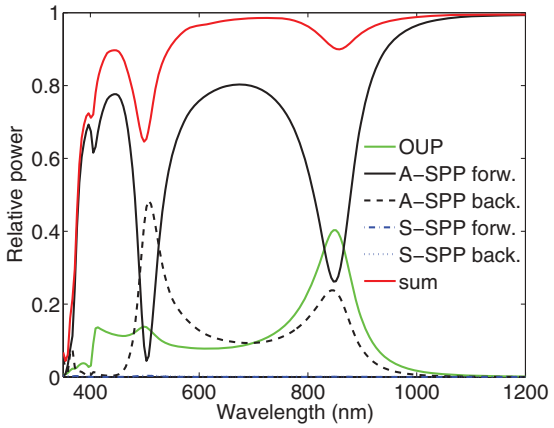

FIG. 4. (Color online) Fraction of power scattered, transmitted, or reflected into each propagating mode channel, and their sum, for the situation in Fig. 1(b) with geometry parameters $w = 100$ nm, $d = 10$ nm, $g = 10$ nm, and $t = 15$ nm, and with an A-SPP as the incident wave.

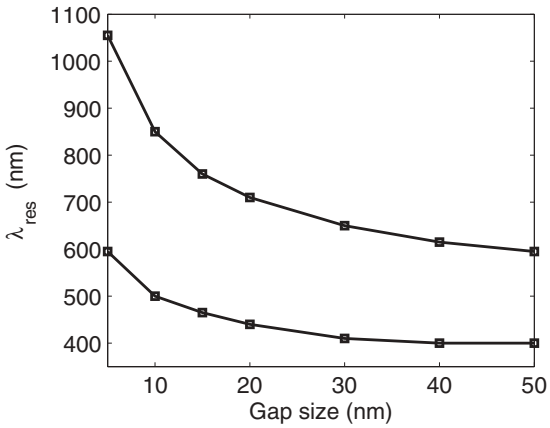

FIG. 5. Resonance wavelengths as a function of gap size g for the structure in Fig. 1 with structure parameters $w = 100$ nm, $d = 10$ nm, and $t = 15$ nm.

wavelengths where we found a scattering resonance before, that is, at the wavelengths 850 and 500 nm. At the same wavelengths we notice a peak in the fraction of power reflected into the backward propagating A-SPP, and we also notice a peak in the fraction of power scattered into OUP waves. Again, the fraction of power coupled into the S-SPP channels is practically negligible. We also notice from the sum of normalized powers in all propagating channels (Fig. 4) that there is a dip at those resonance wavelengths implying that there is resonant absorption as well as resonant scattering. For the very short wavelengths around 400 nm we notice a very large absorption which is due to an extremely small propagation length of the A-SPP and large absorption in the silver. For the resonance wavelength 850 nm approximately 40% of the A-SPP incident power is coupled out from the A-SPP and into OUP waves. It is remarkable that such a high fraction of light can be coupled out from the A-SPP with only one nanostrip of this small size.

As before, the resonances are related to standing-wave resonances of gap-SPP waves in the gap between nanostrip and metal film. The resonance wavelengths depend on the gap-SPP propagation constant and reflection phase at strip terminations, and thus the resonance wavelengths will depend on the size of the gap g between the nanostrip and film. In particular the mode index $n_{\text{gap-SPP}} = k_{\text{gap-SPP}}/k_0$ of the gap-SPP wave decreases with increasing gap size g. From previous work[46,47,53–55] we expect that the resonance wavelengths are given approximately by the relation

$$\text{Re}(n_{\text{gap-SPP}})\frac{2\pi}{\lambda}2w + \phi_R = m2\pi, \qquad (11)$$

where ϕ_R is the total round-trip reflection phase for a gap-SPP being reflected at both the left and the right nanostrip terminations, and m is an integer. Thus, when $n_{\text{gap-SPP}}$ decreases the resonance wavelength must also decrease, and thus increasing the gap g will result in a blue shift of the resonance wavelength. The resonance wavelength for the two resonances as a function of gap size is presented in Fig. 5. The overall behavior is in accordance with our interpretation of resonances being standing-wave gap-SPP resonances and Eq. (11).

In order to quantify the effect of Ohmic losses for at least one case we have made a calculation similar to Fig. 4 where the Ohmic loss of silver was neglected, that is, the imaginary part of the silver dielectric constant was set to zero (Fig. 6). The sum of the fraction of powers from all propagating-wave channels is now unity. The resonance wavelengths are practically the same as with Ohmic losses included (Fig. 4), but resonances are slightly sharper and are characterized by smaller resonant transmission and larger resonant reflection and scattering. Qualitatively the calculations with and without loss are similar.

For the case with absorption losses we have obtained the resonance wavelengths from calculations similar to Fig. 4 for a wide range of strip widths w for a fixed gap size $g = 10$ nm (Fig. 7). The result is in agreement with what can be expected from Eq. (11), namely that the resonance wavelength is approximately proportional to the strip width w with a proportionality factor depending on the resonance order m.

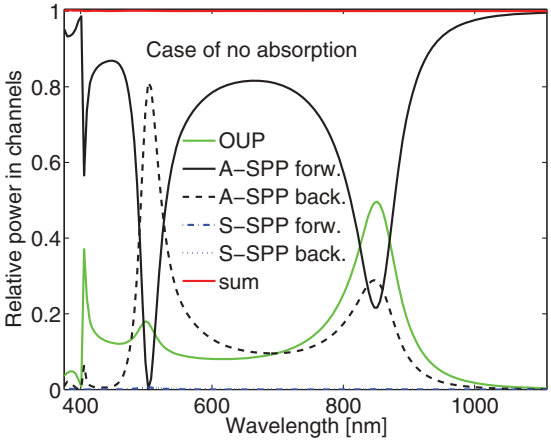

FIG. 6. (Color online) The same calculation as in Fig. 4 except that Ohmic losses in the silver were neglected.

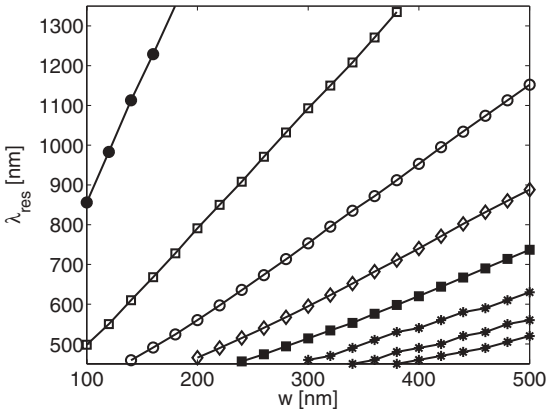

FIG. 7. Resonance wavelengths versus strip width w for the structure in Fig. 1 with structure parameters $d = 10$ nm, $t = 15$ nm, and $g = 10$ nm.

It is possible to extract the round-trip reflection phase ϕ_R (modulo 2π) by inserting the data in Fig. 7 into Eq. (11). A similar procedure was previously used to obtain the reflection phase for metal nanostrip resonators,[58] where it was found that the result depends slightly on the order m of the resonance considered. The calculation of ϕ_R for different orders m for our case is shown in Fig. 8. It is very important for this calculation that the resonance wavelengths inserted into Eq. (11) are accurate, and thus the results in Fig. 8 were obtained with a 1-nm wavelength resolution. The value of ϕ_R is clearly strongly wavelength dependent, which means that in general it is not straightforward to use Eq. (11) to predict the resonance wavelengths since the correct round-trip phase is usually not known. However, the differences in ϕ_R obtained for different m are small enough that Eq. (11) describes the main physics of the resonances. In order to calculate the reflection phase unambiguously (without m dependence) it is necessary to consider a semi-infinite geometry (along x) so that only a single reflection at a single geometry termination is considered, similar to what was done in Refs. 59 and 60 for other geometries.

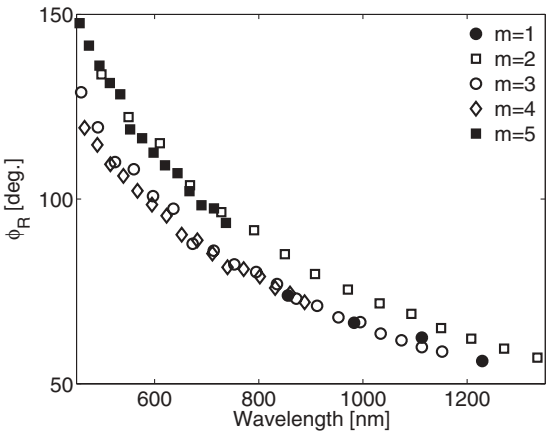

FIG. 8. Total round-trip reflection phase for the resonant geometry (Fig. 1) with structure parameters $d = 10$ nm, $t = 15$ nm, and $g = 10$ nm, obtained by inserting the data in Fig. 7 into Eq. (11).

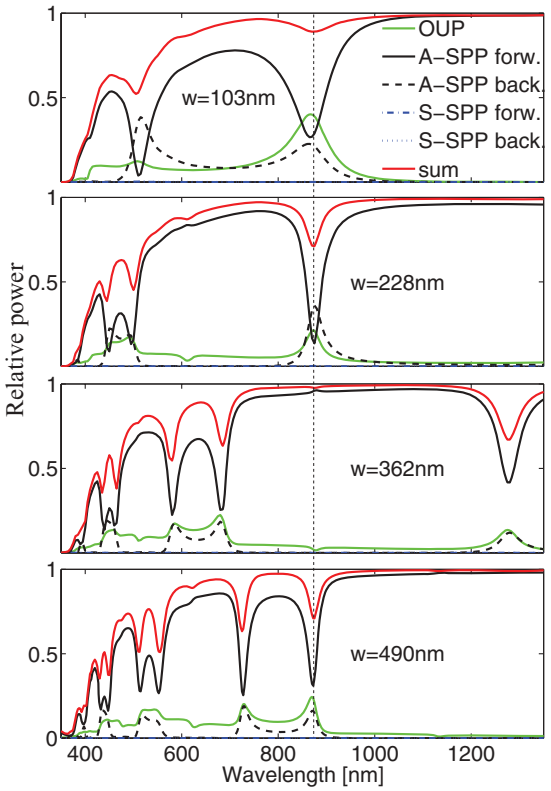

FIG. 9. (Color online) Fraction of power scattered, transmitted, or reflected into each propagating mode channel, and their sum, for the situation in Fig. 1(b) with geometry parameters $d = 10$ nm, $g = 10$ nm, and $t = 15$ nm, and with an A-SPP as the incident wave, for strip widths $w = 103$, 228, 362, and 490 nm.

Returning to Fig. 7 we can see that for the investigated range of strip widths there are four strip widths resulting in a resonance wavelength of approximately 875 nm. The scattering calculation for the situation in Fig. 1(b) with an A-SPP as incident wave for these four different strip widths of $w = 103$, 228, 362, and 490 nm, is shown in Fig. 9. Here the strip is centered at $x = 0$, and the powers in the respective A-SPP and S-SPP waves are evaluated at $x = \pm 251$ nm. Notice that the increase in strip width between the different resonance orders is approximately the same, and approximately matches a half wavelength for a gap-SPP wave primarily confined to the 10-nm gap between a 10-nm silver film and a 15-nm silver film ($\lambda_{\text{gap-SPP}}/2 = \lambda/n_{\text{gap-SPP}}/2 = 875$ nm$/3.39/2 = 129$ nm, where $n_{\text{gap-SPP}}$ was obtained with a transfer-matrix method similar to the one described in Ref. 54). Also notice that the power scattered into forward and backward propagating S-SPPs is still negligible. While some of the resonances are only just seen in Fig. 9 they can still be clearly identified from plots of the electric field magnitude in the gap (Figs. 10 and 11).

We have also made similar calculations to the situation in Fig. 1(b) but with an S-SPP as the incident wave (not shown). In that case practically all power was transmitted into the forward propagating S-SPP with negligible coupling to A-SPP and OUP waves. Actually, we have found that the fractions of power coupled from an incident S-SPP to forward and backward propagating A-SPPs are exactly the same as

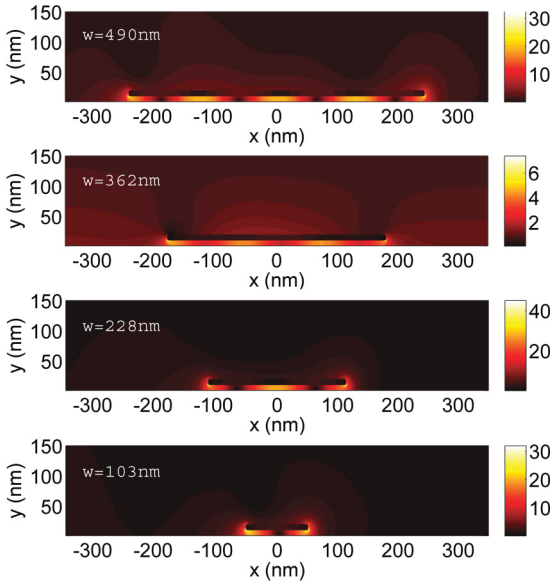

FIG. 10. (Color online) Normalized magnitude of electric field around the nanostrip for the situations considered in Fig. 9 at the resonance wavelength 875 nm for the four considered strip widths w.

the fractions of power coupled from an incident A-SPP to forward and backward propagating S-SPPs. This also serves as a numerical check since this result follows directly from reciprocity.

IV. SCATTERING BY A HIGH OBJECT ABOVE A 15-NM-THIN FILM

In this section we will consider if it is possible to couple light into and out from S-SPP waves by replacing the 10-nm-thick nanostrip with a much higher object. This can be motivated from the knowledge that while overall a magnetic line dipole will emit less light into both A-SPP waves and S-SPP waves with increasing distance to the film then there is a crossover distance above which it will emit more light into the S-SPP wave than into the A-SPP wave.[49]

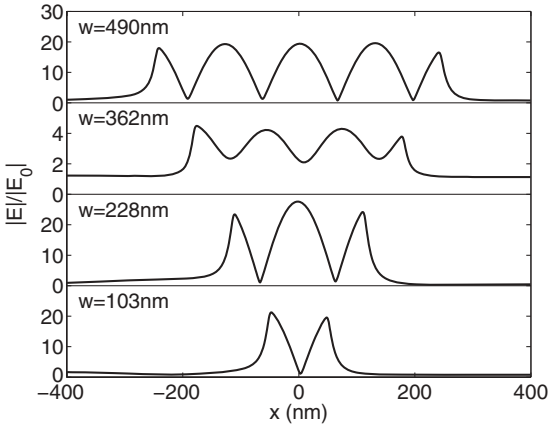

FIG. 11. Cross sections of the normalized field magnitude through the center of the gap between metal strip and metal film ($y = 5$ nm) for the field plots in Fig. 10.

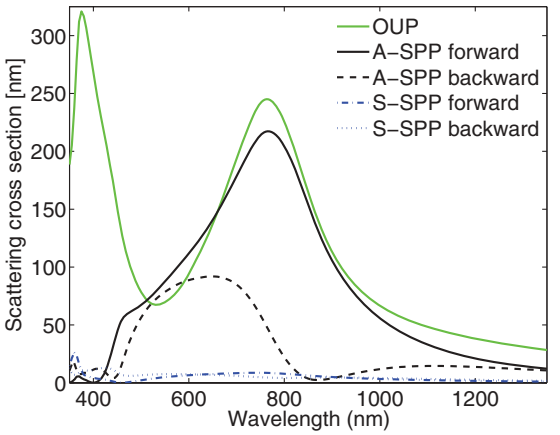

FIG. 12. (Color online) Channel specific scattering cross sections for the situation in Fig. 1(a) with $w = 100$ nm, $d = 100$ nm, $g = 10$ nm, and $t = 15$ nm. The angle of light incidence is 45°.

The first case we will consider is the situation in Fig. 1(a) with parameters $t = 15$ nm, $g = 10$ nm, $w = 100$ nm, and $d = 100$ nm (Fig. 12). Compared with Fig. 2 with a 10-nm-thick strip we observe here for a 100-nm-thick object at least a noticeable amount of light coupled from the plane wave and into the forward and backward propagating S-SPP waves. However, the coupling of light into A-SPP waves is still much more significant than the coupling to S-SPP waves. For the wavelength of approximately 765 nm, where both the OUP and forward A-SPP cross sections peak, we notice that the OUP and forward propagating A-SPP scattering cross sections are similar in value with a comparatively small scattering into backward propagating A-SPPs. Thus, scattering into A-SPPs can be both efficient and directional.

The case of the scattering situation similar to Fig. 1(b) but with an S-SPP as the incident wave is considered in Fig. 13. Here the power in the different SPP channels is evaluated 1 nm to the left or to the right of the scattering object. In this case the S-SPP forward channel (transmission) increases with the

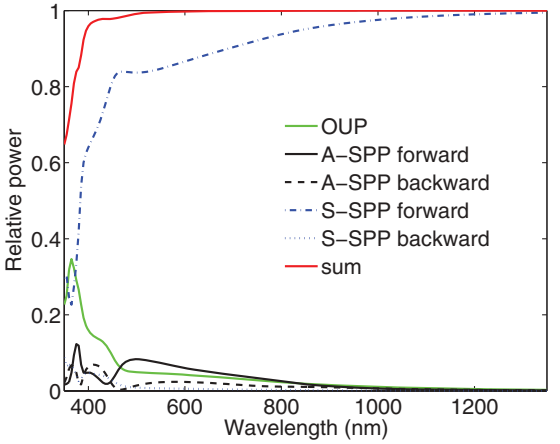

FIG. 13. (Color online) Fraction of power scattered, transmitted, or reflected into each propagating mode channel, and their sum, for the situation in Fig. 1(b) with geometry parameters $w = 100$ nm, $d = 100$ nm, $g = 10$ nm, and $t = 15$ nm, and with an S-SPP as the incident wave.

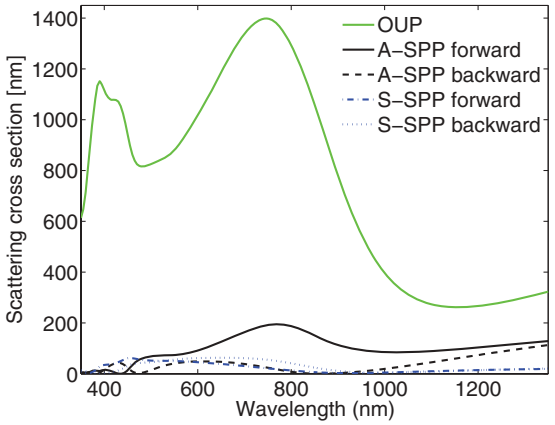

FIG. 14. (Color online) Channel specific scattering cross sections for the situation in Fig. 1(a) with $w = 100$ nm, $d = 500$ nm, $g = 10$ nm, and $t = 15$ nm. The angle of light incidence is 45°.

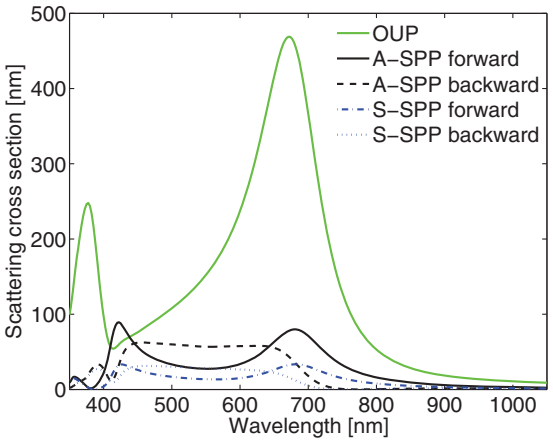

FIG. 16. (Color online) Channel specific scattering cross sections for the situation in Fig. 1(a) with $w = 100$ nm, $d = t = 50$ nm, and $g = 10$ nm. The angle of light incidence is 45°.

wavelength in accordance with the S-SPP becoming weaker bound to the film with increasing wavelength, and thus the scattering object will become smaller compared with the size of the S-SPP for increasing wavelengths. A small fraction of the incident S-SPP power is coupled to OUP waves and A-SPP waves, and except for the shortest of the considered wavelengths with the strongest S-SPP confinement only very little power is reflected into the backward propagating S-SPP.

Since we got at least a noticeable amount of power coupled into and out from the S-SPP by using a higher scattering object we will try to increase the height further to $d = 500$ nm. Similar calculations for this height of the scatterer are presented in Figs. 14 and 15. The scattering cross section related to S-SPP waves did increase but not compared with the corresponding increase in the OUP scattering cross section. A major effect now is that the OUP scattering cross section is always also significantly larger than the A-SPP scattering cross sections which was not the case with the 10-nm-high (Fig. 2) and 100-nm-high (Fig. 12) scattering objects. Thus, overall, a 500-nm-high scattering object does not seem useful for efficient coupling of light from a plane wave and into SPP waves.

The coupling from an incident S-SPP into all propagating wave channels with the 500-nm-high object is considered in Fig. 15. Compared with the smaller object heights then the transmission (S-SPP forward) is reduced, and it is clear that the most important channel into which power is transferred from the incident S-SPP is the OUP wave channel. Thus, while it appears to be problematic to efficiently couple light into S-SPP waves then, at least for the shorter of the considered wavelengths, light can be efficiently coupled out from the S-SPP wave and into OUP propagating waves.

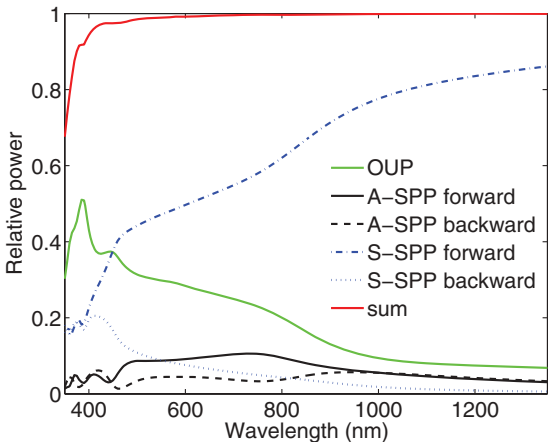

FIG. 15. (Color online) Fraction of power scattered, transmitted, or reflected into each propagating mode channel, and their sum, for the situation similar to Fig. 1(b) but with an S-SPP as the incident wave, and with geometry parameters $w = 100$ nm, $d = 500$ nm, $g = 10$ nm, and $t = 15$ nm.

V. SCATTERING BY AN OBJECT PLACED ABOVE A 50-NM-THIN FILM

In this section we consider using a thicker metal film ($t = 50$ nm) to increase the S-SPP scattering cross section and the coupling of light out of the S-SPP. As the film thickness increases the S-SPP will become stronger bound to the metal film and the A-SPP will become weaker bound. This can be seen from the confinement lengths that for the wavelength 500 nm are $L_{\text{S-SPP}} = 304$ nm and $L_{\text{A-SPP}} = 182$ nm, and for the wavelength 1350 nm they are $L_{\text{S-SPP}} = 2562$ nm and $L_{\text{A-SPP}} = 1705$ nm. In the limit of infinite film thickness the A-SPP and S-SPP propagation constants and confinement lengths are identical and equal to the corresponding values of a single-metal-dielectric-interface SPP. Thus, increasing the film thickness reduces the difference between A-SPPs and S-SPPs.

The first case we will consider (Fig. 16) is the scattering situation in Fig. 1(a) with geometry parameters $d = t = 50$ nm, $g = 10$ nm, and $w = 100$ nm. Clearly the A-SPP scattering cross sections are still larger than the S-SPP cross sections but not by more than a factor of 2. Notice the similar spectral dependence of A-SPP and S-SPP cross sections. For the scattering situation similar to Fig. 1(b) but with an S-SPP incident on the same nanostrip (Fig. 17) we notice, for example, for the wavelength 650 nm that the S-SPP transmission (S-SPP forward) is approximately 83% with approximately 10% of the power redirected to OUP waves,

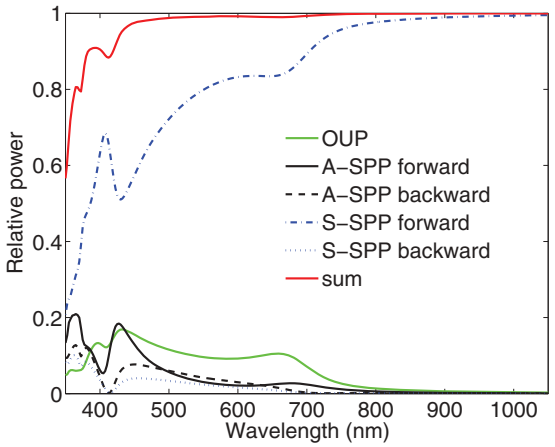

FIG. 17. (Color online) Fraction of power scattered, transmitted, or reflected into each propagating mode channel, and their sum, for the situation similar to Fig. 1(b) but with an S-SPP as the incident wave, and with geometry parameters $w = 100$ nm, $d = t = 50$ nm, and $g = 10$ nm.

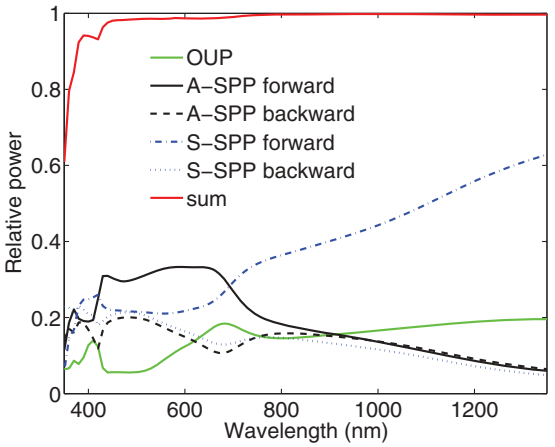

FIG. 19. (Color online) Fraction of power scattered, transmitted, or reflected into each propagating mode channel, and their sum, for the situation similar to Fig. 1(b) but with an S-SPP as the incident wave, and with geometry parameters $w = 100$ nm, $d = 700$ nm, $t = 50$ nm, and $g = 10$ nm.

which means that a significant amount of the power which is not transmitted is coupled to OUP waves.

For completeness we also consider an A-SPP as the incident wave in the same geometry (Fig. 18). We notice a similarity in the overall behavior of the curves with that found for the S-SPP as incident wave but with more absorption, larger out-coupling from the A-SPP compared with that found for the S-SPP, etc. The qualitative similarity of the curves in Figs. 17 and 18 reflects that the A-SPP and S-SPP properties are more similar now with the film thickness of 50 nm than what was the case for the 15-nm film thickness. Note that the curves in Fig. 17 showing the coupling from the S-SPP forward propagating wave to A-SPP forward and backward propagating waves are in fact identical to the curves in Fig. 18 showing the coupling from the A-SPP forward propagating wave to S-SPP forward and backward propagating waves. This result follows also directly from reciprocity.

As a final example we will consider an S-SPP incident on a large scattering object extending significantly above the metal film with thickness $d = 700$ nm and $w = 100$ nm, again with a gap $g = 10$ nm to the metal film of thickness $t = 50$ nm (Fig. 19). Naturally one effect of the large scattering object is that the transmission (S-SPP forward) is reduced for the whole wavelength range considered and no longer approaches unity for the longest of the considered wavelengths. For wavelengths smaller than 900 nm the main channel for redistribution of the power upon scattering is into the forward propagating A-SPP. Scattering into the backward propagating S-SPP and A-SPP are similar. For the longer wavelengths beyond 900 nm the OUP scattering channel contains more power than the other scattering channels and increasingly more so with increasing wavelength. For wavelengths between approximately 400 and 700 nm more light is scattered into the forward propagating A-SPP than is transmitted into the forward propagating S-SPP.

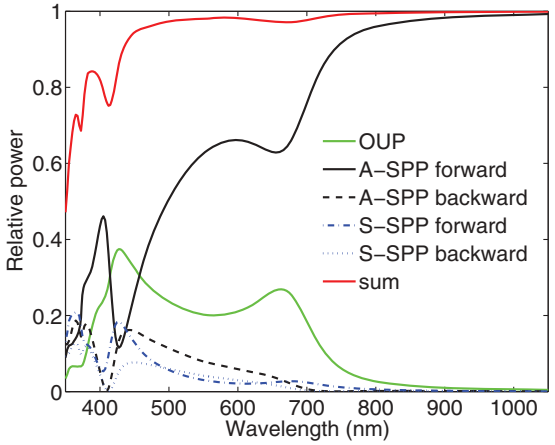

FIG. 18. (Color online) The same as Fig. 17 except that the incident wave is an A-SPP.

VI. CONCLUSION

In this paper we considered scattering by a silver nanostrip placed near a nanometer-thin silver film supporting both symmetric and antisymmetric SPP waves. For a 15-nm-thin silver film and a nanostrip of thickness 10 nm, widths in the range from 100 to 500 nm, and at distances of 10 to 50 nm from the film, scattering resonances were observed both with plane-wave illumination and with A-SPP illumination that could be explained as a consequence of excitation of standing-wave gap-SPP resonances in the gap between metal film and metal nanostrip. For such a geometry the excitation of symmetric SPP waves with both methods of illumination was negligible, and practically all scattered power was redirected to forward or backward propagating A-SPP waves or out-of-plane propagating waves. The total A-SPP scattering cross section, including both forward and backward propagating A-SPPs, could exceed the OUP scattering cross section at resonance, making in-coupling from a plane wave to A-SPP waves efficient, and reversely, at resonance, more than 40% of the A-SPP power could be coupled out into OUP

propagating waves with a single scatterer of width approximately 100 nm.

Different strategies for improving the in-coupling to and out-coupling from S-SPP waves were pursued including using a higher scattering object and a larger film thickness. Larger scattering objects with thicknesses of 100 and 500 nm led to a noticeable but still small in-coupling to S-SPP waves compared with the other scattering channels. For a 500-nm-high object the main channel for out-coupling of light from the S-SPP was into OUP propagating waves, such that while S-SPP waves are difficult to excite it is not so difficult to couple light out from them. By increasing the film thickness to 50 nm the scattering cross section for S-SPP waves was now not more than a factor of 2 smaller than the A-SPP scattering cross sections and display a qualitatively similar spectral dependence. Also, with either an S-SPP or A-SPP as the incident wave we found that the spectra for the relative power transmitted, reflected, and scattered into SPP waves of opposite symmetry or into OUP propagating waves were qualitatively similar, reflecting that the A-SPP and S-SPP properties are more similar for the thicker film.

ACKNOWLEDGMENTS

T.S. and J.J. gratefully acknowledge the financial support from the project "Localized-surface plasmons and silicon thin-film solar cells - PLATOS" financed by the Villum foundation. Furthermore, T.S. acknowledges that this work was carried out with financial support from the Danish Agency for Science, Technology and Innovation, as part of the project Active Nano Plasmonics (ANAP, FTP-Project No. 09-072949).

*ts@nano.aau.dk

[1] H. Raether, *Surface Plasmons on Smooth and Rough Surfaces and on Gratings* (Springer, New York, 1986).
[2] J. J. Burke, G. I. Stegeman, and T. Tamir, Phys. Rev. B **33**, 5186 (1986).
[3] E. N. Economou, Phys. Rev. **182**, 539 (1969).
[4] D. Sarid, Phys. Rev. Lett. **47**, 1927 (1981).
[5] J. Jung, T. Søndergaard, and S. I. Bozhevolnyi, Phys. Rev. B **76**, 035434 (2007).
[6] P. Berini, Phys. Rev. B **61**, 10484 (2000).
[7] P. Berini, Opt. Lett. **24**, 1011 (1999).
[8] P. Berini, Opt. Express **7**, 327 (2000).
[9] P. Berini, R. Charbonneau, N. Lahoud, and G. Mattiussi, J. Appl. Phys. **98**, 043109 (2005).
[10] S. J. Al-Bader, IEEE J. Quantum Electron. **40**, 325 (2004).
[11] R. Charbonneau, C. Scales, I. Breukelaar, S. Fafard, N. Lahoud, G. Mattiussi, and P. Berini, J. Lightwave Technol. **24**, 477 (2006).
[12] K. Leosson, T. Nikolajsen, A. Boltasseva, and S. I. Bozhevolnyi, Opt. Express **14**, 314 (2006).
[13] J. A. Dionne, L. A. Sweatlock, H. A. Atwater, and A. Polman, Phys. Rev. B **72**, 075405 (2005).
[14] A. Degiron, S.-Y. Cho, T. Tyler, N. M. Jokerst, and D. R. Smith, New J. Phys. **11**, 015002 (2009).
[15] A. Boltasseva and S. I. Bozhevolnyi, J. Sel. Top. Quantum Electron. **12**, 1233 (2006).
[16] A. Boltasseva, T. Nikolajsen, K. Leosson, K. Kjaer, M. S. Larsen, and S. I. Bozhevolnyi, J. Lightwave Technol. **23**, 413 (2005).
[17] A. Boltasseva, S. I. Bozhevolnyi, T. Søndergaard, T. Nikolajsen, and K. Leosson, Opt. Express **13**, 4237 (2005).
[18] T. Søndergaard, S. I. Bozhevolnyi, and A. Boltasseva, Phys. Rev. B **73**, 045320 (2006).
[19] A. Boltasseva, T. Søndergaard, T. Nikolajsen, K. Leosson, and J. M. Hvam, J. Opt. Soc. Am. B **22**, 2027 (2005).
[20] W. Mu, D. B. Buchholz, M. Sukharev, J. I. Jang, R. P. H. Chang, and J. B. Ketterson, Opt. Lett. **35**, 550 (2010).
[21] P. Mühlschlegel, H.-J. Eisler, O. J. F. Martin, B. Hecht, and D. W. Pohl, Science **308**, 1607 (2005).
[22] L. Novotny and N. van Hulst, Nat. Photon. **5**, 83 (2011).
[23] L. Novotny, Phys. Today **64**, 47 (2011).
[24] T. Søndergaard and S. I. Bozhevolnyi, Phys. Rev. B **75**, 073402 (2007).
[25] E. S. Barnard, J. S. White, A. Chandran, and M. L. Brongersma, Opt. Express **16**, 16529 (2008).
[26] P. Biagioni, J.-S. Huang, and B. Hecht, Rep. Prog. Phys. **75**, 024402 (2012).
[27] D. Zhang, X. Yuan, and A. Bouhelier, Appl. Opt. **49**, 875 (2010).
[28] S. Massenot, J. Grandidier, A. Bouhelier, G. Colas des Francs, L. Markey, J.-C. Weeber, A. Dereux, J. Renger, M. U. González, and R. Quidant, Appl. Phys. Lett. **91**, 243102 (2007).
[29] A. Drezet, A. Hohenau, D. Koller, A. Stepanov, H. Ditlbacher, B. Steinberger, F. R. Aussenegg, A. Leitner, and J. R. Krenn, Mater. Sci. Eng. B **149**, 220 (2008).
[30] M. Böhmler, N. Hartmann, C. Georgi, F. Hennrich, A. A. Green, M. C. Hersam, and A. Hartschuh, Opt. Express **18**, 16443 (2010).
[31] E. Skovsen, T. Søndergaard, J. Fiutowski, H.-G. Rubahn, and K. Pedersen, J. Opt. Soc. Am B **29**, 249 (2012).
[32] J. Kalkman, H. Gersen, L. Kuipers, and A. Polman, Phys. Rev. B **73**, 075317 (2006).
[33] I. Gryczynski, J. Malicka, W. Jiang, H. Fischer, W. C. W. Chan, Z. Gryczynski, W. Grudzinski, and J. R. Lakowicz, J. Phys. Chem. B **109**, 1088 (2005).
[34] H. Ditlbacher, J. R. Krenn, N. Felidj, B. Lamprecht, G. Schider, M. Salerno, A. Leitner, and F. R. Aussenegg, Appl. Phys. Lett. **80**, 404 (2002).
[35] F. López-Tejeira, S. G. Rodrigo, L. Martín-Moreno, F. J. García-Vidal, E. Devaux, T. W. Ebbesen, J. R. Krenn, I. P. Radko, S. I. Bozhevolnyi, M. U. González, J. C. Weeber, and A. Dereux, Nat. Phys. **3**, 324 (2007).
[36] C. Ropers, C. C. Neacsu, T. Elsaesser, M. Albrecht, M. B. Raschke, and C. Lienau, Nano Lett. **7**, 2784 (2007).
[37] I. P. Radko, S. I. Bozhevolnyi, G. Brucoli, L. Martín-Moreno, F. J. García-Vidal, and A. Boltasseva, Phys. Rev. B **78**, 115115 (2008).
[38] F. López-Tejeira, S. G. Rodrigo, L. Martín-Moreno, F. J. García-Vidal, J. Dintinger, T. W. Ebbesen, J. R. Krenn, I. P. Radko, S. I. Bozhevolnyi, M. U. González, J. C. Weeber, and A. Dereux, New. J. Phys. **10**, 033035 (2008).
[39] J. A. Sánchez-Gil, Appl. Phys. Lett. **73**, 3509 (1998).
[40] J. A. Sánchez-Gil, Opt. Lett. **28**, 2255 (2003).

[41] A. V. Shchegrov, I. V. Novikov, and A. A. Maradudin, Phys. Rev. Lett. **78**, 4269 (1997).
[42] A. Yu. Nikitin, G. Brucoli, F. J. García-Vidal, and L. Martín-Moreno, Phys. Rev. B **77**, 195441 (2008).
[43] F. López-Tejeira, F. J. García-Vidal, and L. Martín-Moreno, Phys. Rev. B **72**, 161405 (2005).
[44] A. Yu. Nikitin, F. López-Tejeira, and L. Martín-Moreno, Phys. Rev. B **75**, 035129 (2007).
[45] G. Brucoli and L. Martín-Moreno, Phys. Rev. B **83**, 045422 (2011).
[46] J. Jung and T. Søndergaard, Phys. Rev. B **77**, 245310 (2008).
[47] J. Jung, T. Søndergaard, and S. I. Bozhevolnyi, Phys. Rev. B **79**, 035401 (2009).
[48] I. Chremmos, J. Opt. Soc. Am. A **27**, 85 (2010).
[49] V. Siahpoush, T. Søndergaard, and J. Jung, Phys. Rev. B **85**, 075305 (2012).
[50] D. Marcuse, *Theory of Dielectric Optical Waveguides* (Academic, New York, 1974).
[51] A. E. Siegmann, Appl. Phys. B: Lasers Opt. **60**, 247 (1995).
[52] P. B. Johnson and R. W. Christy, Phys. Rev. B **6**, 4370 (1972).
[53] T. Søndergaard, J. Jung, S. I. Bozhevolnyi, and G. Della Valle, New J. Phys. **10**, 105008 (2008).
[54] T. Søndergaard and S. I. Bozhevolnyi, Phys. Status Solidi B **245**, 9 (2008).
[55] A. Chandran, E. S. Barnard, J. S. White, and M. L. Brongersma, Phys. Rev. B **85**, 085416 (2012).
[56] H. T. Miyazaki and Y. Kurokawa, Appl. Phys. Lett. **89**, 211126 (2006).
[57] H. T. Miyazaki and Y. Kurokawa, Phys. Rev. Lett. **96**, 097401 (2006).
[58] T. Søndergaard, J. Beermann, A. Boltasseva, and S. I. Bozhevolnyi, Phys. Rev. B **77**, 115420 (2008).
[59] R. Gordon, Phys. Rev. B **73**, 153405 (2006).
[60] R. Gordon, Phys. Rev. B **74**, 153417 (2006).